ADVANCED FUNCTIONAL MATERIALS
www.afm-journal.de

# Core/Shell Perovskite Nanocrystals: Synthesis of Highly Efficient and Environmentally Stable $FAPbBr_3/CsPbBr_3$ for LED Applications

*Chengxi Zhang, Sheng Wang, Xiaomin Li, Mingjian Yuan, Lyudmila Turyanska,* and Xuyong Yang**

**Lead halide perovskite nanocrystals (PeNCs) are promising materials for applications in optoelectronics. However, their environmental instability remains to be addressed to enable their advancement into industry. Here the development of a novel synthesis method is reported for monodispersed PeNCs coated with all inorganic shell of cesium lead bromide ($CsPbBr_3$) grown epitaxially on the surface of formamidinium lead bromide ($FAPbBr_3$) NCs. The formed $FAPbBr_3/CsPbBr_3$ NCs have photoluminescence in the visible range 460–560 nm with narrow emission linewidth (20 nm) and high optical quantum yield, photoluminescence quantum yield (PLQY) up to 93%. The core/shell perovskites have enhanced optical stability under ambient conditions (70 d) and under ultraviolet radiation (50 h). The enhanced properties are attributed to overgrowth of $FAPbBr_3$ with all-inorganic $CsPbBr_3$ shell, which acts as a protective layer and enables effective passivation of the surface defects. The use of these green-emitting core/shell $FAPbBr_3/CsPbBr_3$ NCs is demonstrated in light-emitting diodes (LEDs) and significant enhancement of their performance is achieved compared to core only $FAPbBr_3$-LEDs. The maximum current efficiency observed in core/shell NC LED is 19.75 cd $A^{-1}$ and the external quantum efficiency of 8.1%, which are approximately four times and approximately eight times higher, respectively, compared to core-only devices.**

## 1. Introduction

The newly emerged lead halide perovskite nanocrystals (PeNCs) have drawn extensive attention owing to their tunable optical properties, narrow emission bandwidth, and high photoluminescence quantum yield (PLQY) and were successfully used in a range of optoelectronic devices such as photodetectors[1] and light-emitting diodes (LEDs).[2–10] However, their inherent instability and degradation of the PLQY over time limit further advance of PeNCs in practical applications. Furthermore, ionic nature presents significant drawback as the PeNCs are extremely sensitive to environmental conditions, particularly to exposure to moisture, oxygen-rich atmosphere, and light.[11,12] Currently intensive research efforts focused on development of synthesis methods and postsynthesis treatments,[13,14] aiming to enhance their stability by modification of crystal structure and chemical composition.[13] Most promising approaches include embedding of PeNCs into a solid matrix[15–20] and surface modification of PeNCs with more stable capping ligands, such as silica and alumina coating[15,17] and polymer matrices.[16] However, presence of these insulating matrices limits uses of the PeNCs in applications requiring charge transfer from the nanocrystals, such as LEDs and photovoltaic devices. Recently significant enhancement of the stability for all-inorganic cesium lead bromide perovskite ($CsPbBr_3$) was achieved by overgrowing the NCs with $TiO_2$ shell;[18] however, the stability of organic–inorganic NCs remains to be addressed. Of particular interest is growth of optically active all-inorganic perovskite shell over organic-containing PeNCs, which has not yet been explored and could bring significant improvements to the optical stability of these NCs. The two materials, $CsPbBr_3$ and formamidinium lead bromide ($FAPbBr_3$), have different lattice structures with lattice mismatch of 3.4%,[6,21,22] presenting challenges for their use in core/shell structure.

Here we report on development of strategy for synthesis of monodispersed perovskite nanocrystals capped with all inorganic shell of $CsPbBr_3$ grown epitaxially on the surface of

Dr. C. X. Zhang, Dr. S. Wang, X. Li, Prof. X. Yang
Key Laboratory of Advanced Display and System Applications of Ministry of Education
Shanghai University
149 Yanchang Road, Shanghai 200072, China
E-mail: yangxy@shu.edu.cn

Prof. M. Yuan
College of Chemistry
Nankai University
94 Weijin Road, Tianjin 300071, China

Dr. L. Turyanska
Faculty of Engineering
University of Nottingham
Nottingham NG7 2RD, UK
E-mail: Lyudmila.Turyanska@nottingham.ac.uk

The ORCID identification number(s) for the author(s) of this article can be found under https://doi.org/10.1002/adfm.201910582.



**DOI: 10.1002/adfm.201910582**

$FAPbBr_3$ NCs. The growth of a layer of alloyed $FA_xCs_{1-x}PbBr_3$ is used to address lattice mismatch between the core and the shell. After the formation of the core/shell structure, the surface of NC core is effectively passivated reducing the number of surface defects. By adjusting the synthesis conditions and composition of the nanocrystals we achieve stable PLQYs of up to 93% for $FAPbBr_3/CsPbBr_3$ core/shell NCs grown with molar ratio of Cs: FA = 1:1. The presence of $CsPbBr_3$ shell over $FAPbBr_3$ NCs leads to better environmental stability, with PLQY maintained at ≈ 80% of its initial value under long term (70 d) storage in ambient conditions. We also note that the core/shell NCs have remarkable stability under continuous irradiation with the ultraviolet (UV) light for at least 50 h, retaining QY of ≈75%. We demonstrate that these core/shell NCs can be used as emitters in LEDs with highly efficient electroluminescent performance. The achieved maximum current efficiency (CE) and external quantum efficiency (EQE) are 19.75 cd $A^{-1}$ and 8.1%, respectively. The results demonstrated here offer realistic prospects for utilization of core/shell perovskite NCs in optoelectronics.

## 2. Results and Discussion

Colloidal $FAPbBr_3$ NCs were synthesized by hot-injection method at $T = 130$ °C following a method adopted from ref. [23]. To overgrow the $FAPbBr_3$ NCs with shell of $CsPbBr_3$ we develop a facile wet-chemical approach, where different amounts of precursor materials ($Cs_2CO_3$, $PbBr_2$) and long-chain capping ligands (oleic acid (OA) and oleylamine (OLA)) and 1-octadecene (ODE) are injected into the solution of preformed $FAPbBr_3$ NCs. The resulting solution is heated to 80 °C in an inert atmosphere for 20 min. We vary the molar ratio, *X*, of Cs to FA with $X = 0.25$, 0.5, 1.0, 1.5, to produce core/shell structures with difference shell thickness (**Figure 1**). Following growth, the nanocrystals are purified with ethyl acetate and finally dissolved in toluene. The samples are stored in the dark at $T = 5$ °C.

Our morphological studies show that the $FAPbBr_3$ NCs have cubic shape with an average size of 8.2 ± 1.2 nm and have uniform composition (**Figure 2**a,b). The high-resolutionv transmission electron microscopy (HRTEM) revealed the crystals

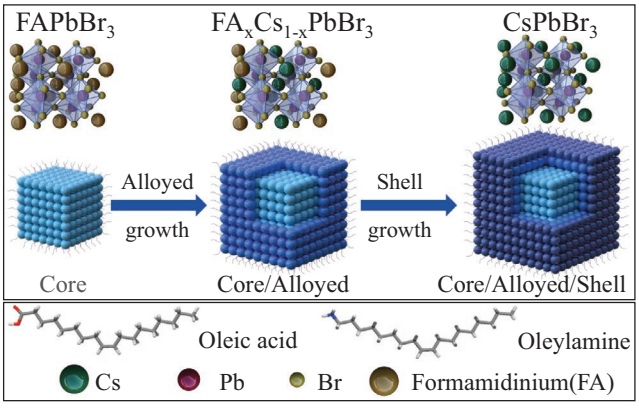


**Figure 1.** Schematic illustration of the lattice structure and the synthesis of core $FAPbBr_3$ NCs and core/alloyed-shell $FAPbBr_3/FA_xCs_{1-x}PbBr_3$ and core/alloyed-shell/shell $FAPbBr_3/FA_xCs_{1-x}PbBr_3/$ $FAPbBr_3/CsPbBr_3$ perovskite NCs.

spacing of about 3.0 Å, characteristic for (200) crystal face of $FAPbBr_3$ cube[1,24,25] (Figure 2c and Figure S1, Supporting Information). The overgrowth of inorganic shell leads to an increase of the average size of the nanocrystals to 11.2 ± 1.1 nm for $X = 1.0$ (Figure 2d), indicating the formation of shell with thickness of ≈1.5 nm. The core–shell NCs retain cubic shape with well-defined edges and corners, indicating better crystallinity and lower defect density. The $FAPbBr_3/CsPbBr_3$ PeNCs have homogeneous composition, with uniform distribution of all elements throughout the NCs (Figure 2e and Figure S2, Supporting Information). After epitaxial overgrowth, the lattice spacing is slightly reduced to 2.9 Å, likely due to internal stress (Figure 2f). Meanwhile, X-ray photoelectron spectroscopy (XPS) revealed a presence of two different peaks with the binding energy of Cs at 723.7 and 737.8 eV, in addition to characteristic peaks of element C 1s, N 1s, Pb 4f, and Br 3d, confirming its incorporation into the lattice[26] (see Figure S3, Supporting Information). XPS spectra of $FAPbBr_3$ NCs, $CsPbBr_3$ NCs, and $FAPbBr_3/CsPbBr_3$ core/shell NCs reveal a general trend of an increase of the amount of Cs, which is accompanied by an increase of the amount of Br.

X-ray diffraction (XRD) spectroscopy was performed to further investigate the structural characteristics of the NCs with and without $CsPbBr_3$ shell (Figure 2i). The $FAPbBr_3$ NCs have the primary diffraction peaks at 14.8°, 21.1°, and 29.8°, which are assigned to the (100), (110), and (200) planes of cubic PeNCs. Following overgrowth with all-inorganic $CsPbBr_3$ shell the diffraction peaks of $FAPbBr_3/CsPbBr_3$ NCs shift toward higher angles with increasing molar ratio of Cs: FA from 0.25 to 1.0. The observed shape of the characteristic peaks becomes similar to those expected for $CsPbBr_3$ for NCs grown with Cs:FA ratio of 1.0 and 1.5. We note that the signals of alloyed perovskite NCs are not observed. This gradual change can be well explained by Vegard's law,[27,28] hence we suggest that a transition layer of the $FA_xCs_{1-x}PbBr_3$ alloy is formed (Figure 1).

The UV–vis absorbance and PL spectra ($\lambda_{ex}$ = 365 nm) for PeNCs at room temperature (RT) are shown in **Figure 3**a. Our $FAPbBr_3$ NCs have an absorption band edge at 520 nm and a narrow PL emission line centered at 532 nm with an full wavelength at half maximum (FWHM) of 21 nm. After shell overgrowth, optical properties of the NCs change and a blueshift is observed with increasing shell thickness: for $X = 1.5$ the PL peak is centered at 504 nm and the FWHM is reduced by ≈3 n m. The gradual changes of optical properties corroborate our XRD findings and support our hypothesis of the formation of alloyed transition layer between organic–inorganic core and all-inorganic shell, hence reducing effective core size to ≈6 nm.[23] We envisage that Cs incorporates into $FAPbBr_3$ crystal reducing the Br–Pb–Br angle and causing a reduction of Pb–Br orbital overlap.[29] We also note that the PL emission of $FAPbBr_3/CsPbBr_3$ core–shell NCs is distinctly different from that of $FA_xCs_{1-x}PbBr_3$ NCs (the two samples are prepared under the same reaction condition and with the same raw stoichiometric ratio, see Section SI1 and Figure S4, Supporting Information). For alloyed $FA_xCs_{1-x}PbBr_3$ NCs we observe significant blueshift and broadening of the PL spectra compared to core–shell NCs. The blueshift of the PL emission peaks in the core–shell NCs is attributed to the formation of alloyed layer of $FA_xCs_{1-x}PbBr_3$ at the core–shell interface of NCs, resulting in reduced effective

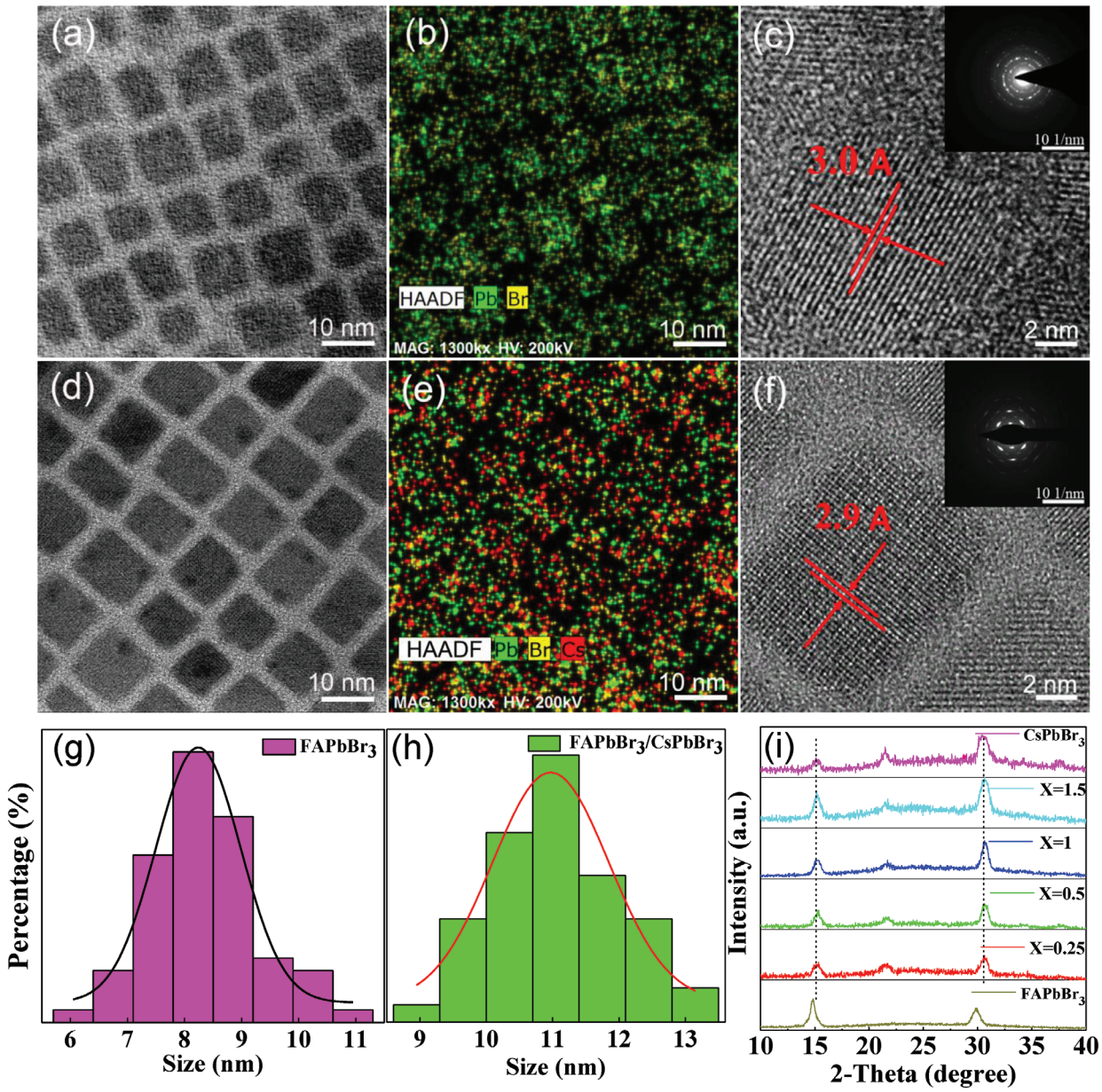


**Figure 2.** Morphological and structural properties of core $FAPbBr_3$ NCs and $FAPbBr_3/CsPbBr_3$ core/shell NCs ($X = 1.0$). a) High-angle annular dark field-scanning transmission electron microscopy (HAADF-STEM) image and b) corresponding elemental mapping image showing the elemental distribution of Pb and Br for $FAPbBr_3$ NCs. c) HRTEM image of a typical $FAPbBr_3$ NC and corresponding selected area electron diffraction (SAED) pattern (inset). d) HAADF-STEM image and e) corresponding elemental mapping image showing the elemental distribution of Pb, Br, and Cs for $FAPbBr_3/CsPbBr_3$ NCs. f) HRTEM image of a typical $FAPbBr_3/CsPbBr_3$ NC and corresponding SAED pattern (inset). g,h) Size distribution analysis for the samples in (a) and (d), respectively. i) XRD patterns of $FAPbBr_3$ NCs, $CsPbBr_3$ NCs, and a series of thickness-controlled $FAPbBr_3/CsPbBr_3$ core/shell NCs (The values of $X$ are the different molar ratio of Cs/FA).

$FAPbBr_3$ core size.[30] Meanwhile, the long-range, infinite lattice periodicity of a core NC is disturbed during the shell coating, and the differences of dielectric constant and absorption coefficient between the core and shell also affect the physical properties of the PeNCs. Hence, we conclude that with the increasing Cs content, the all-inorganic shell of $CsPbBr_3$ is formed over the transitional alloyed layer. The observed blueshift is consistent with increasing strength of exciton confinement in $FAPbBr_3$ for NCs capped with a thicker shell of $CsPbBr_3$. Importantly, by overgrowing the NCs with inorganic shell we increase the PLQY reaching a maximum value of 93% for $X = 1.0$ (inset in Figure 3a). In order to understand the dynamics of carrier recombination, we study the time-resolved PL (Figure 3b). The decay times can be fitted well-with a biexponential function (Equation (1))[31,32]

$$A(t) = A_1 \exp\left(\frac{-t}{\tau_1}\right) + A_2 \exp\left(\frac{-t}{\tau_2}\right) \quad (1)$$

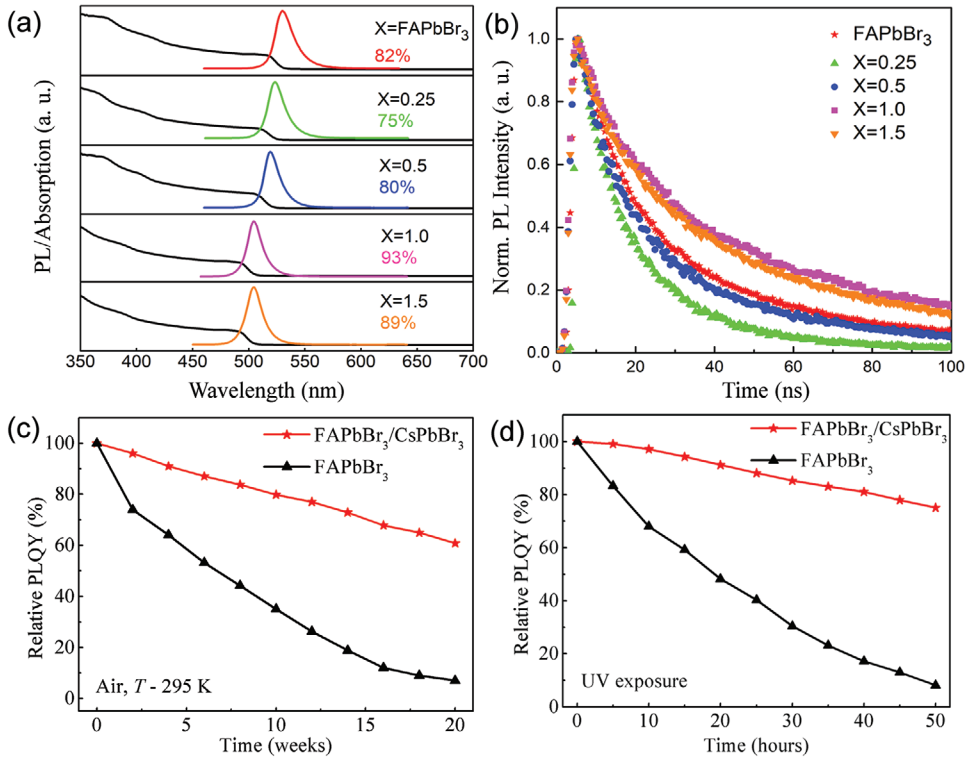


**Figure 3.** a) UV–vis absorbance and PL spectra and b) time-resolved PL decay curves of $FAPbBr_3$ NCs and $FAPbBr_3/CsPbBr_3$ NCs with different thickness-controlled (The values of *X* are the different molar ratio of Cs/FA and other values are the corresponding quantum yields). Time dependence of relative PLQY of core only and core/shell NCs c) under storage in ambient conditions and d) under exposure to 365 nm UV light.

where $A_1$ and $A_2$ are constants, $t$ is time, and $\tau_1$ represents the trap-assisted recombination at grain boundaries and $\tau_2$ is ascribed to radiative recombination (see Table S1, Supporting Information). We find that with increasing *X*, corresponding to increasing shell thickness, the PL lifetime of $FAPbBr_3/CsPbBr_3$ NCs exhibits the same trend as that of PLQYs, with $\tau_{av}$ value increased from 30.2 ns of $FAPbBr_3$ NCs to 40.1 ns of $FAPbBr_3/CsPbBr_3$ NCs (at $X = 1.0$). These observations confirm that the shell overgrowth provides more efficient passivation of surface defects on $FAPbBr_3$ NCs hence reducing the number of nonradiative recombination centers.

The long-term stability of the NCs is of paramount importance for their application in optoelectronic devices. Hence, we examine the shelf life of the core/shell NCs. We find that storage of the NCs in ambient conditions (air and room temperature) (Figure 3c) leads to significant decrease of the relative PLQY of $FAPbBr_3$ NCs to <10% over 20 weeks, while $FAPbBr_3/CsPbBr_3$ NCs retain PLQY > 60%. The core/shell NCs also demonstrate enhanced stability under UV illumination ($\lambda = 365$ nm), retaining over 80% of original PLQY, compared to <20% for core only NCs, following 50 h exposure (Figure 3d). Overall, we found that the stability of PeNCs with core/shell structure is significantly improved compared to bare NCs.

Formation of core/shell perovskite NCs was further confirmed by our temperature dependent PL studies (80–300 K) (**Figure 4**a,b). With increasing temperature, we observe a blueshift of PL peak position by 74 meV for $FAPbBr_3$ NCs with gradients of 0.3 meV $K^{-1}$, characteristic for this type of materials.[33,34] In contrast, the PL peak of $FAPbBr_3/CsPbBr_3$ core/shell NCs blueshifts by ≈30.6 meV, with gradient of 0.3 meV K at $T < 150$ K and 0.6 meV $K^{-1}$ at higher temperature. The observed difference of temperature dependence of the optical energy gap confirms presence of a shell providing stronger exciton confinement. The *T*-dependent blueshift of optical bandgap is common for perovskite NCs and was observed for $CH_3NH_3PbX_3$ and $Cs_3Sb_2Br_9$ PeNCs.[35,36] With increasing *T*, the integrated PL intensity decreases due to the thermally activated nonradiative recombination processes (Figure 4c). We estimated the exciton binding energy ($E_b$) from o temperature-dependent PL spectra by following equation[37]

$$I(T) = \frac{I_0}{1 + A\exp\left(-\frac{E_b}{K_B T}\right)} \quad (2)$$

where $I_o$ is the emission intensity at low temperature, *A* is a constant, and $K_B$ is the Boltzmann constant. From our curve fitting we find $E_b \approx 51$ meV for $FAPbBr_3$ NCs and $E_b = 64$ meV for $FAPbBr_3/CsPbBr_3$ core/shell NCs. The observed increase of ≈130% confirms stronger binding of the exciton in core/shell NCs. The optical linewidth (Figure 4c) of the $FAPbBr_3/CsPbBr_3$ NCs is FWHM = 115 meV at RT, which is significantly broader compared to core-only $FAPbBr_3$ NCs (90 meV), which we attribute to a decrease of the strength of exciton-phonon coupling for core/shell NCs.[36]

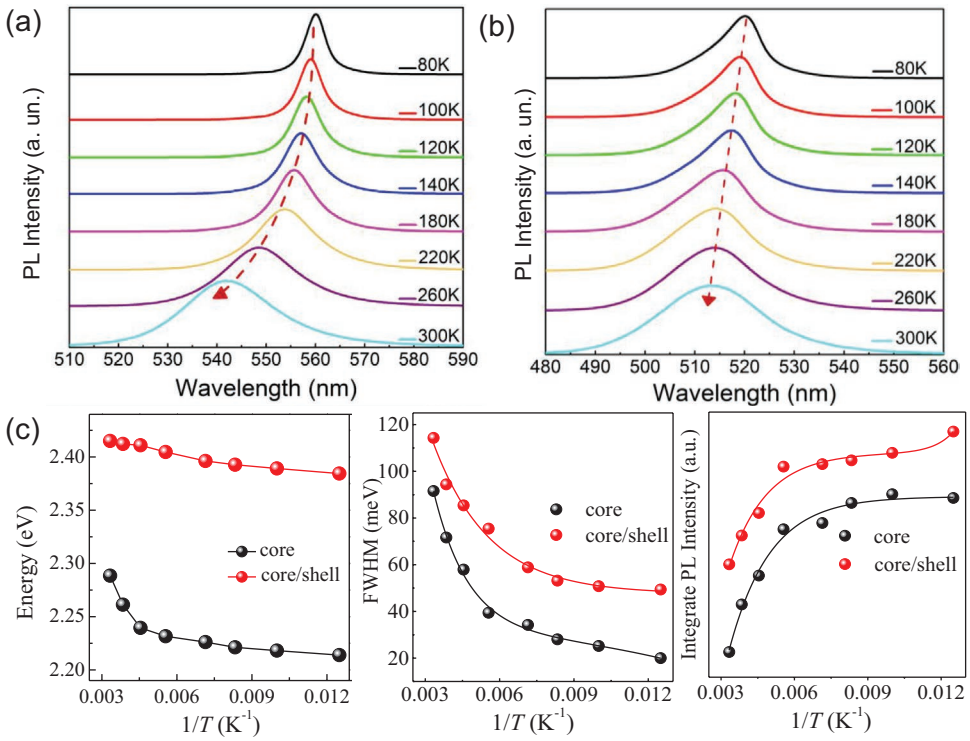


**Figure 4.** Temperature-dependent PL spectra of a) $FAPbBr_3$ NCs and b) $FAPbBr_3/CsPbBr_3$ (molar ratio Cs:FA = 1.0). c) Temperature dependence of PL peak position, PL linewidth, and integrated PL intensity for $FAPbBr_3$ NCs and $FAPbBr_3/CsPbBr_3$ (Cs/FA = 1.0).

Enhanced optical properties and environmental stability of the core–shell NCs could offer exciting prospects for their exploitation in optoelectronic devices. Hence, we produce LED structures with a layer of $FAPbBr_3$ NCs or $FAPbBr_3/CsPbBr_3$ core/shell NCs. (**Figure 5**a,b, see also Section SI1 and Table S2, Supporting Information). The perovskite LED (PeLED) consists of multilayers of an indium tin oxide (ITO) anode, poly(3,4-ethyllenedioxythiophene)-polystyrene sulfonate (PEDOT:PSS) hole injection layer (HIL), poly(*N*,*N*′-bis(4-butylphenyl)-*N*,*N*′-bis(phenyl)-benzidine) (poly-TPD) hole transport layer (HTL), a PeNCs emission layer, 1,3,5-tris(1-phenyl-1H-benzimidazol-2yl) benzene (TPBI) electron transport layer, LiF electron injection layer, and Al cathode. Poly-TPD is used as an HTL and electron-blocking interlayer simultaneously due to its low electron affinity (≈2.2 eV) and high hole mobility, which is matched to that of TPBI (both around $1 \times 10^{-4}$ $cm^2$ $V^{-1}$ $s^{-1}$).[38,39] Figure 5c shows normalized electroluminescence (EL) spectra of PeLEDs based on $FAPbBr_3/CsPbBr_3$ core/shell NCs with different values of *X*. We observe a blueshift of EL peak position from 536 to 508 nm with *X* increasing from 0 to 1.5, similar to that observed for PL peak (see Section SI2 and Figure S4, Supporting Information). We note that the separation between EL and PL peak positions decreases with increasing *X*, likely due to lower defect density, which is consistent with observed increase of PLQY.

We also examine the effect of washing on device performance (see Table S3, Supporting Information). We find the highest value of EQE with two repeats of washing for device fabricated with both core and core–shell NCs. Notably, up to ten-time increase in the EQE is observed for devices based on core–shell NCs. Hence we select the NCs with best performance for further studies. The current density–voltage (*J*–*V*), luminance–voltage (*L*–*V*), and current efficiency–current density (CE–*J*) curves of these devices are shown in Figure 5d–f. The device based on core-only $FAPbBr_3$ NCs has a luminance of 1593 cd $m^{-2}$ and CE of 4.80 cd $A^{-1}$. With increasing shell thickness (*X* = 0.25, 0.5, and 1.0) of core/shell NCs, the CE and EQE gradually increase to 19.75 cd $A^{-1}$ and 8.1% (*X* = 1.0), respectively. However, further increase of *X* to 1.5 leads to a decrease of the luminance of PeLEDs from 1758 to 957 cd $m^{-2}$ and the CE has reduced to 7.76 cd $A^{-1}$ (see also **Table 1**). We observe the maximum CE and EQE for the NCs with *X* = 1.0 and these values are fourfold and eightfold higher compared to those of the bare $FAPbBr_3$-based PeLEDs. We also noted that the PeLEDs based on core/shell NCs show a greatly improved operational lifetime compared with the $FAPbBr_3$-based PeLEDs due to the better optical stability of the NCs (see Figure S5, Supporting Information). The device parameters achieved in our work with $FAPbBr_3$ NCs overgrown with inorganic shell are better or comparable to those recently reported for hybrid perovskite LEDs.[40,41] These results confirm that the core/shell NCs can be used as an effective emitting layer in high performance PeLEDs with additional benefit of long shelf life.

## 3. Conclusion

In conclusion, we have developed an epitaxial growth method for the overgrowth of $CsPbBr_3$ shell on the surface of $FAPbBr_3$ NCs. The formed core/shell $FAPbBr_3/CsPbBr_3$ NCs have improved PLQY (93%) and long-term shelf life and optical

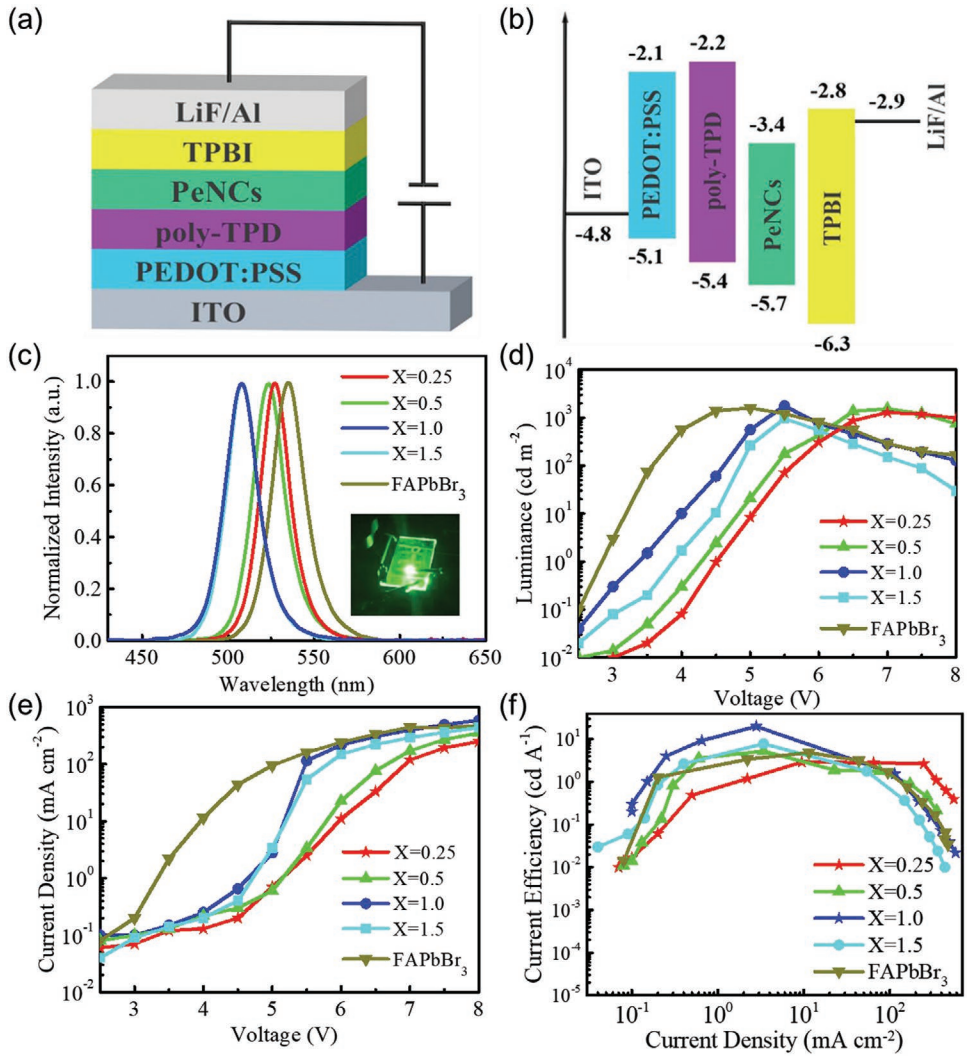


**Figure 5.** a) Device structure of the PeLEDs. b) Energy diagram of the PeLEDs. The PeNCs energy level values were determined by ultraviolet photoelectron spectroscopy (UPS) measurements (see Table S2, Supporting Information) and other functional layers are obtained from refs. [42,43]. c) EL spectra. Inset: A working device ($X$ = 1.0 with an emitting area of 2 mm × 2 mm) at an applied voltage of 5.5 V. d) Current density–voltage. e) Luminance–voltage and f) current efficiency–current density curves of the PeLEDs based on different molar ratio of Cs/FA.

stability under UV illumination. We attribute the enhanced optical and environmental stability to effective passivation of the surface defects and hence increase radiative recombination. We demonstrated that the PeLEDs based on the $FAPbBr_3/CsPbBr_3$ core/shell NCs (Cs/FA = 1.0) have improved performance compared to those fabricated with core-only NCs, with maximum CE of 19.75 cd $A^{-1}$, EQE of 8.1%, which is almost 4.1-fold, 7.9-fold higher than that of the bare $FAPbBr_3$-based PeLEDs. Notably, this work can open new avenues for the NC design and is relevant for their utilization in high-efficiency luminescent flat panel display applications.

**Table 1.** Performance parameters of $FAPbBr_3/CsPbBr_3$ core/shell based LEDs prepared with NCs with different molar ratio, $X$, of Cs:FA.

| Molar ratio FA: Cs, $X$ | $L_{max}$ [cd $m^{-2}$] | $CE_{max}$ [cd $A^{-1}$] | $EQE_{max}$ [%] | $V_{on}$ [V] |
|---|---|---|---|---|
| 0.25 | 1281 | 2.89 | 0.59 | 2.9 |
| 0.5 | 1528 | 5.22 | 1.29 | 2.8 |
| 1.0 | 1758 | 19.75 | 8.10 | 2.6 |
| 1.5 | 957 | 7.76 | 3.18 | 3.0 |
| 0 | 1593 | 4.80 | 1.03 | 2.5 |

## 4. Experimental Section

*Synthesis of Perovskite Nanocrystals*: All reagents were purchased and used without further purification: FA-acetate (Sigma-Aldrich), $Pb(CH_3COO)_2 \times 3H_2O$ (Sinopharm Chemical Reagent Co., Ltd., ≥99.5%), octadecene (ODE, Sigma-Aldrich, 90%), OA (Sigma-Aldrich, 90%), OAmBr (Xi'an Polymer Light Technology Crop), toluene (Sinopharm Chemical Reagent Co., Ltd., ≥99.5%), $PbBr_2$ (Sigma-Aldrich, 90%), $Cs_2CO_3$ (Sigma-Aldrich), OLA (Sigma-Aldrich, 90%).

$FAPbBr_3$ NCs were synthesized as following method reported in ref. [23]. Briefly, FA-acetate (0.078 g, 0.75 mmol), $Pb(CH_3COO)_2 \cdot 3H_2O$ (0.076 g, 0.2 mmol), OA (2 mL, vacuum dried at 120 °C), and ODE (8 mL, vacuum-dried at 120 °C) were combined in a 100 mL and dried for 30 min under vacuum at 50 °C. The mixture was heated to 130 °C

under $N_2$ atmosphere and OAmBr (0.21 g, 0.6 mmol) in toluene (2 mL) was injected. After 10 s, the reaction mixture was cooled on ice-water bath. The green solution of $FAPbBr_3$ NCs was collected and stored at $T = 4$ °C.

For synthesis of $FAPbBr_3/CsPbBr_3$ nanocrystals, $PbBr_2$ (0.1101 g, 0.3 mmol) and $Cs_2CO_3$ (0.0326 g, 0.1 mmol) were loaded into a 100 mL flask. Then, dried OA (1 mL), dried ODE (5 mL), dried OLA (0.5 mL), and as synthesized $FAPbBr_3$ nanocrystals (12 mL) were added. The mixture was heated to 80 °C for 20 min under $N_2$ atmosphere, followed by cooling on ice bath. The color of the reaction solution has changed significantly compared to the original solution of $FAPbBr_3$ NCs. Finally, the resulting solution was centrifuged to remove undispersed residue and aggregated nanocrystals. The $FAPbBr_3/CsPbBr_3$ NCs dispersed in hexane were stored in the dark at $T = 4$ °C.

*Purification*: As-prepared crude solution of $FAPbBr_3$ and $FAPbBr_3/CsPbBr_3$ NCs was put into centrifuge tubes and a certain volume of ethyl acetate was added (keeping the volume ratio of crude solution to ethyl acetate 1:3), then centrifuged at 7000 rpm for 5 min. After that, the precipitate was redissolved in *n*-hexane and centrifuged for 1 min at 5000 rpm. Finally, the supernatant was collected and stored at 4 °C. This is the PeNC solution after a purification, according to the actual test requirements or application needs, which can be purified twice or three times (see Table S3, Supporting Information).

*Characterization Methods*: Transmission electron microscope Talos F200X was used to assess the morphology, size distribution, and elements composition of the NCs. XRD patterns were recorded on a Bruker D8 Advance diffractometer with Cu $K_\alpha$ radiation range from 10° to 60° at a scanning rate of 4° $min^{-1}$. UV–vis absorption spectra were measured on Hitachi J-3900H spectrometer. The photoluminescence (PL) spectra and time-resolved fluorescence were measured on Edinburgh FLS920 spectrometer. Temperature dependence of PL was measured on a Princeton Instruments Acton SP2750.

*Device Preparation*: PEDOT: PSS (Clevious PVP AI 4083) was purchased from Heraeus. Poly-TPD, TPBI, and LiF were purchased from Luminescence Technology and used without further purification. For device fabrication, the ITO glass was cleaned in ultrasound bath with detergent followed by deionized water, acetone, and isopropyl alcohol (30 min in each solvent). After drying, the substrates were treated in oxygen plasma for 15 min. PEDOT: PSS solutions (filtered through a 0.22 µm filter) were spin coated onto ITO glass at 4000 rpm for 40 s and heated at 150 °C for 10 min. The substrates were transferred into a nitrogen glove box. The poly-TPD solution in chlorobenzene (8 mg $mL^{-1}$) was spin coated at 4000 rpm for 60 s. Then perovskite NCs were spin coated at 2000 rpm for 60 s. Finally, the samples were transferred into a vacuum deposition chamber and TPBI (50 nm) and LiF/Al electrodes (1 nm/100 nm) were sequentially deposited by thermal evaporation at a base pressure of $\approx 4 \times 10^{-4}$ Pa. The current density–luminance–voltage (*J–I–V*) characteristics were measured using Keithley 2400 sourcemeter. The EL spectra were measured on an Ocean Optics 2000 spectrometer.

## Supporting Information

Supporting Information is available from the Wiley Online Library or from the author.

## Acknowledgements

C.Z. and S.W. contributed equally to this work. The authors would like to thank the financial support from National Natural Science Foundation of China (Nos. 51675322, 61605109, and 61735004), National Key Research and Development Program of China (No. 2016YFB0401702), Shanghai Science and Technology Committee (No. 19010500600), Shanghai Rising-Star Program (No. 17QA1401600), Science and Technology Commission of Shanghai Municipality Program (19DZ2281000 and 17DZ2281700), and the Program for Professor of Special Appointment (Eastern Scholar) at Shanghai Institutions of Higher Learning. L.T. acknowledges support from the Engineering and Physical Sciences Research Council [Grant Number EP/P03/1684/1].

## Conflict of Interest

The authors declare no conflict of interest.

## Keywords

core/shell nanocrystals, light-emitting diodes, optical stability, perovskite nanocrystals, quantum efficiency

Received: December 20, 2019
Revised: April 29, 2020
Published online:

[1] D. M. Jang, D. H. Kim, K. Park, J. Park, J. W. Lee, J. K. Song, *J. Mater. Chem. C* **2016**, *4*, 10625.
[2] Z.-K. Tan, R. S. Moghaddam, M. L. Lai, P. Docampo, R. Higler, F. Deschler, M. Price, A. Sadhanala, L. M. Pazos, D. Credgington, F. Hanusch, T. Bein, H. J. Snaith, R. H. Friend, *Nat. Nanotechnol.* **2014**, *9*, 687.
[3] H.-K. Seo, H. Kim, J. Lee, M.-H. Park, S.-H. Jeong, Y.-H. Kim, S.-J. Kwon, T.-H. Han, S. Yoo, T.-W. Lee, *Adv. Mater.* **2017**, *29*, 1605587.
[4] X. Yang, X. Zhang, J. Deng, Z. Chu, Q. Jiang, J. Meng, P. Wang, L. Zhang, Z. Yin, J. You, *Nat. Commun.* **2018**, *9*, 570.
[5] R. L. Z. Hoye, M. R. Chua, K. P. Musselman, G. Li, M.-L. Lai, Z.-K. Tan, N. C. Greenham, J. L. MacManus-Driscoll, R. H. Friend, D. Credgington, *Adv. Mater.* **2015**, *27*, 1414.
[6] Y.-H. Kim, G.-H. Lee, Y.-T. Kim, C. Wolf, H. J. Yun, W. Kwon, C. G. Park, T. W. Lee, *Nano Energy* **2017**, *38*, 51.
[7] Y. H. Kim, H. Cho, H. H. Jin, T. S. Kim, T. W. Lee, *Adv. Mater.* **2015**, *27*, 1248.
[8] M. Yuan, L. N. Quan, R. Comin, G. Walters, R. Sabatini, O. Voznyy, S. Hoogland, Y. Zhao, E. M. Beauregard, P. Kanjanaboos, Z. Lu, D. H. Kim, E. H. Sargent, *Nat. Nanotechnol.* **2016**, *11*, 872.
[9] L. Zhang, X. Yang, Q. Jiang, P. Wang, Z. Yin, X. Zhang, H. Tan, Y. Yang, M. Wei, B. R. Sutherland, E. H. Sargent, J. You, *Nat. Commun.* **2017**, *8*, 15640.
[10] B. T. Diroll, R. D. Schaller, *Adv. Funct. Mater.* **2019**, *29*, 1901725.
[11] J. De Roo, M. Ibáñez, P. Geiregat, G. Nedelcu, W. Walravens, J. Maes, J. C. Martins, I. Van Driessche, M. V. Kovalenko, Z. Hens, *ACS Nano* **2016**, *10*, 2071.
[12] S. Huang, Z. Li, B. Wang, N. Zhu, C. Zhang, L. Kong, Q. Zhang, A. Shan, L. Li, *ACS Appl. Mater. Interfaces* **2017**, *9*, 7249.
[13] H. Han, B. Jeong, T. H. Park, W. Cha, S. M. Cho, Y. Kim, H. H. Kim, D. Kim, D. Y. Ryu, W. K. Choi, C. Park, *Adv. Funct. Mater.* **2019**, *29*, 1970181.
[14] C. Zhang, L. Turyanska, H. Cao, L. Zhao, M. W. Fay, R. Temperton, J. O'Shea, N. R. Thomas, K. Wang, W. Luan, A. Patanè, *Nanoscale* **2019**, *11*, 13450.
[15] C. Sun, Y. Zhang, C. Ruan, C. Yin, X. Wang, Y. Wang, W. W. Yu, *Adv. Mater.* **2016**, *28*, 10088.
[16] S. N. Raja, Y. Bekenstein, M. A. Koc, S. Fischer, D. Zhang, L. Lin, R. O. Ritchie, P. Yang, A. P. Alivisatos, *ACS Appl. Mater. Interfaces* **2016**, *8*, 35523.
[17] Z. Li, L. Kong, S. Huang, L. Li, *Angew. Chem., Int. Ed.* **2017**, *56*, 8134.

[18] Z.-J. Li, E. Hofman, J. Li, A. H. Davis, C.-H. Tung, L.-Z. Wu, W. Zheng, *Adv. Funct. Mater.* **2018**, *28*, 1704288.
[19] B. Wang, C. Zhang, S. Huang, Z. Li, L. Kong, L. Jin, J. Wang, K. Wu, L. Li, *ACS Appl. Mater. Interfaces* **2018**, *10*, 23303.
[20] M.-H. Park, J. Park, J. Lee, H. S. So, H. Kim, S.-H. Jeong, T.-H. Han, C. Wolf, H. Lee, S. Yoo, T.-W. Lee, *Adv. Funct. Mater.* **2019**, *29*, 1902017.
[21] R. Ding, X. Zhang, G. Chen, H. Wang, R. Kishor, J. Xiao, F. Gao, K. Zeng, X. Chen, X. W. Sun, Y. Zheng, *Nano Energy* **2017**, *37*, 126.
[22] S. Kumar, J. Jagielski, N. Kallikounis, Y.-H. Kim, C. Wolf, F. Jenny, T. Tian, C. J. Hofer, Y.-C. Chiu, W. J. Stark, T.-W. Lee, C.-J. Shih, *Nano Lett.* **2017**, *17*, 5277.
[23] L. Protesescu, S. Yakunin, M. I. Bodnarchuk, F. Bertolotti, N. Masciocchi, A. Guagliardi, M. V. Kovalenko, *J. Am. Chem. Soc.* **2016**, *138*, 14202.
[24] M. Imran, V. Caligiuri, M. Wang, L. Goldoni, M. Prato, R. Krahne, L. De Trizio, L. Manna, *J. Am. Chem. Soc.* **2018**, *140*, 2656.
[25] D. N. Minh, J. Kim, J. Hyon, J. H. Sim, H. H. Sowlih, C. Seo, J. Nam, S. Eom, S. Suk, S. Lee, E. Kim, Y. Kang, *Chem. Mater.* **2017**, *29*, 5713.
[26] H. Cho, J. S. Kim, C. Wolf, Y.-H. Kim, H. J. Yun, S.-H. Jeong, A. Sadhanala, V. Venugopalan, J. W. Choi, C.-L. Lee, R. H. Friend, T.-W. Lee, *ACS Nano* **2018**, *12*, 2883.
[27] R. J. Sutton, G. E. Eperon, L. Miranda, E. S. Parrott, B. A. Kamino, J. B. Patel, M. T. Hörantner, M. B. Johnston, A. A. Haghighirad, D. T. Moore, H. J. Snaith, *Adv. Energy Mater.* **2016**, *6*, 1502458.
[28] J. H. Noh, S. H. Im, J. H. Heo, T. N. Mandal, S. I. Seok, *Nano Lett.* **2013**, *13*, 1764.
[29] R. Prasanna, A. Gold-Parker, T. Leijtens, B. Conings, A. Babayigit, H.-G. Boyen, M. F. Toney, M. D. McGehee, *J. Am. Chem. Soc.* **2017**, *139*, 11117.
[30] L. Polavarapu, B. Nickel, J. Feldmann, A. S. Urban, *Adv. Energy Mater.* **2017**, *7*, 1700267.
[31] A. Swarnkar, A. R. Marshall, E. M. Sanehira, B. D. Chernomordik, D. T. Moore, J. A. Christians, T. Chakrabarti, J. M. Luther, *Science* **2016**, *354*, 92.
[32] Z. Liang, S. Zhao, Z. Xu, B. Qiao, P. Song, D. Gao, X. Xu, *ACS Appl. Mater. Interfaces* **2016**, *8*, 28824.
[33] Y. Liu, H. Lu, J. Niu, H. Zhang, S. Lou, C. Gao, Y. Zhan, X. Zhang, Q. Jin, L. Zheng, *AIP Adv.* **2018**, *8*, 095108.
[34] L. Yang, K. Wei, Z. Xu, F. Li, R. Chen, X. Zheng, X. Cheng, T. Jiang, *Opt. Lett.* **2018**, *43*, 122.
[35] J. Zhang, Y. Yang, H. Deng, U. Farooq, X. Yang, J. Khan, J. Tang, H. Song, *ACS Nano* **2017**, *11*, 9294.
[36] J. Xing, F. Yan, Y. Zhao, S. Chen, H. Yu, Q. Zhang, R. Zeng, H. V. Demir, X. Sun, A. Huan, Q. Xiong, *ACS Nano* **2016**, *10*, 6623.
[37] Z. Shi, Y. Li, Y. Zhang, Y. Chen, X. Li, D. Wu, T. Xu, C. Shan, G. Du, *Nano Lett.* **2017**, *17*, 313.
[38] X. Zhang, Y. Zhang, Y. Wang, S. Kalytchuk, S. V. Kershaw, Y. Wang, P. Wang, T. Zhang, Y. Zhao, H. Zhang, T. Cui, Y. Wang, J. Zhao, W. W. Yu, A. L. Rogach, *ACS Nano* **2013**, *7*, 11234.
[39] X. Dai, Z. Zhang, Y. Jin, Y. Niu, H. Cao, X. Liang, L. Chen, J. Wang, X. Peng, *Nature* **2014**, *515*, 96.
[40] Y. Shang, Y. Liao, Q. Wei, Z. Wang, B. Xiang, Y. Ke, W. Liu, Z. Ning, *Sci. Adv.* **2019**, *5*, eaaw8072.
[41] K. Yang, F. Li, H. Hu, T. Guo, T. W. Kim, *Nano Energy* **2019**, *65*, 104029.
[42] Q. Shan, J. Song, Y. Zou, J. Li, L. Xu, J. Xue, Y. Dong, B. Han, J. Chen, H. Zeng, *Small* **2017**, *13*, 1701770.
[43] H. Wang, X. Li, M. Yuan, X. Yang, *Small* **2018**, *14*, 1703410.